

Planetary Remote Sensing Studies of Mars and Moon

Department of Remote Sensing



Seasonal thermal inertia variations at Gale Crater, Mars: Role of active surface deposition phenomena

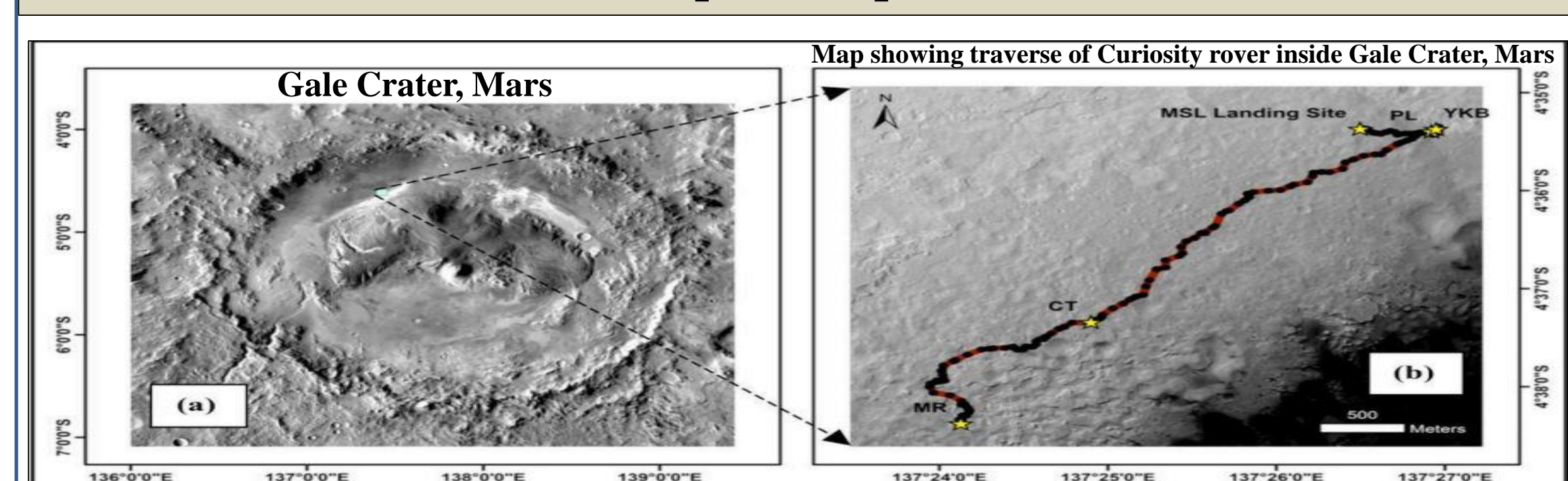


Fig. 1 (a) Gale Crater, Mars (b) Curiosity traverse map showing four locations within Gale Crater – Point Lake (PL), John Klein - Yellowknife Bay (YKB), Cooperstown (CT) and Mt. Remarkable (MR)

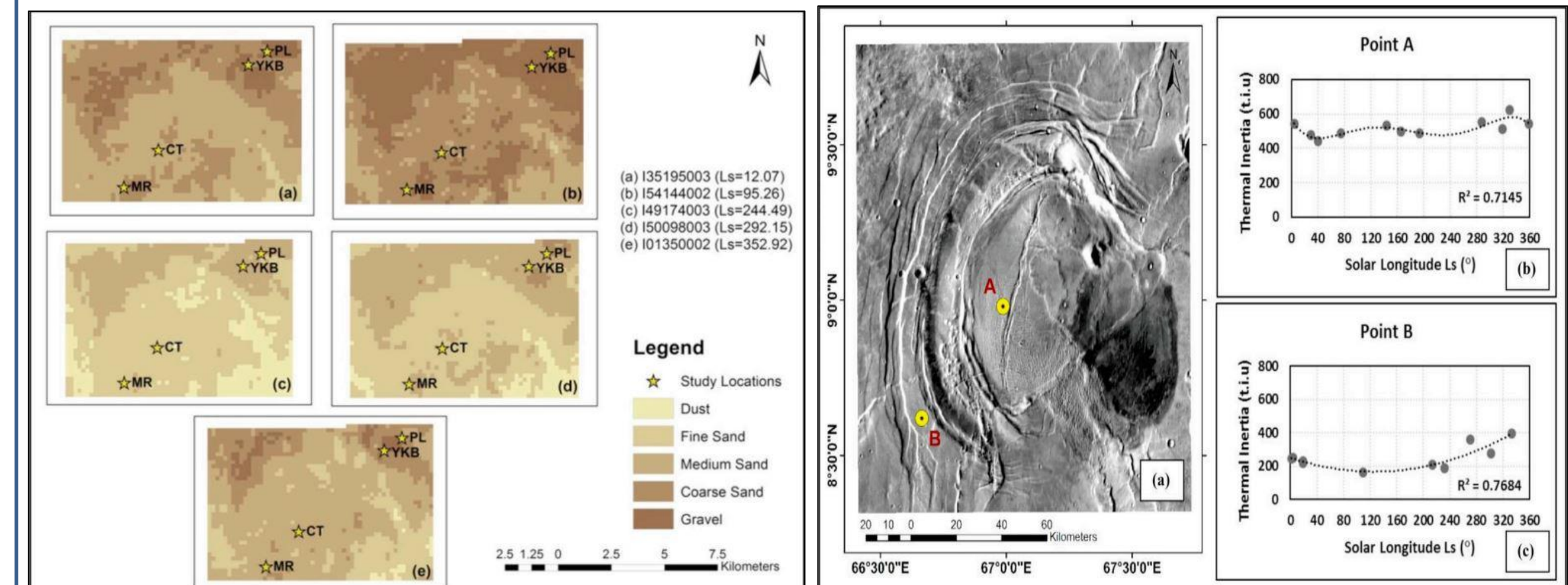


Fig. 2 Particle size distribution maps derived from selected THEMIS (Thermal Emission Imaging System) thermal inertia (TI) images

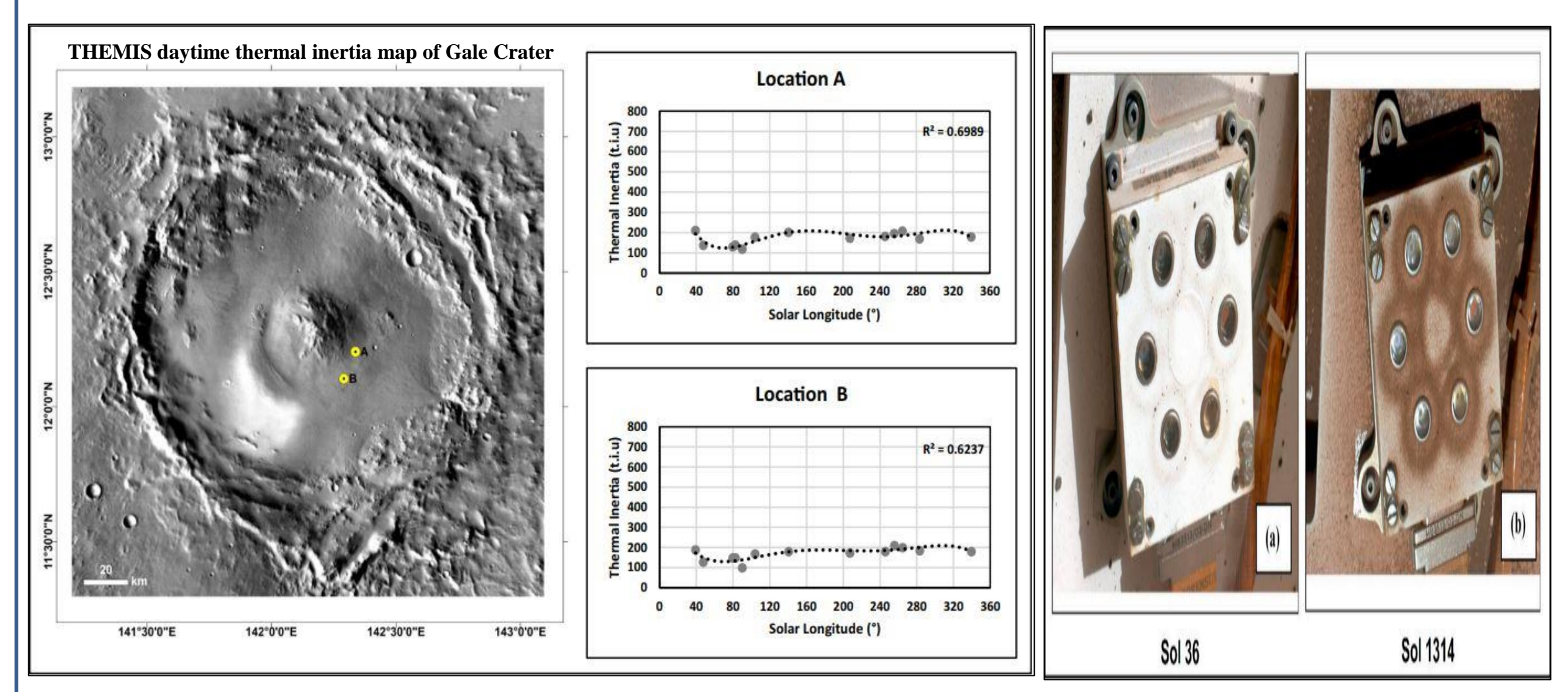


Fig. 3 (a) THEMIS Day Time IR mosaic of the Nili Patera caldera (b) Seasonal TI variation at point A and point C

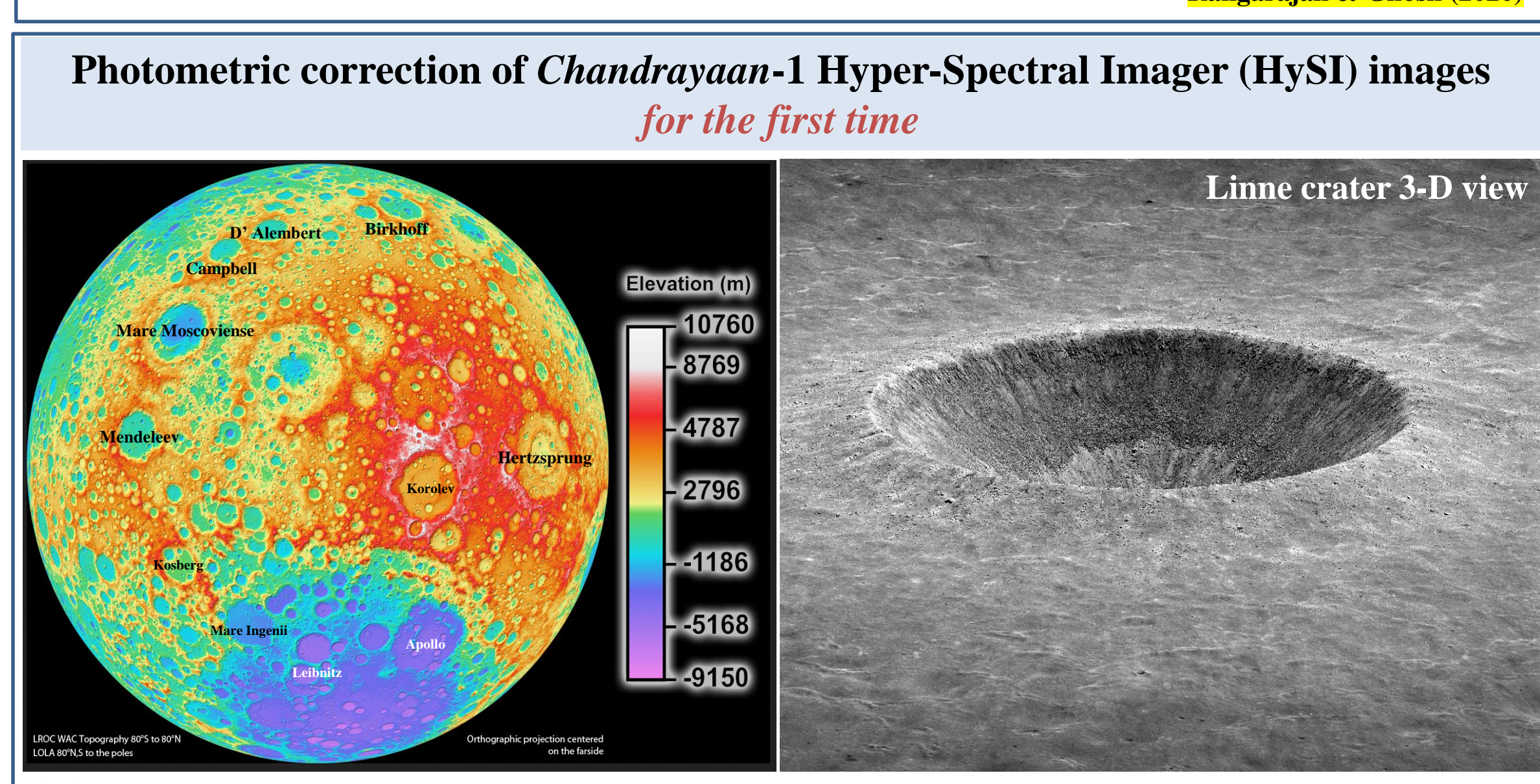


Fig. 4 (a) THEMIS Day Time IR mosaic of Eddie crater (b) Seasonal TI variation at location A (c) Seasonal TI variation at location B

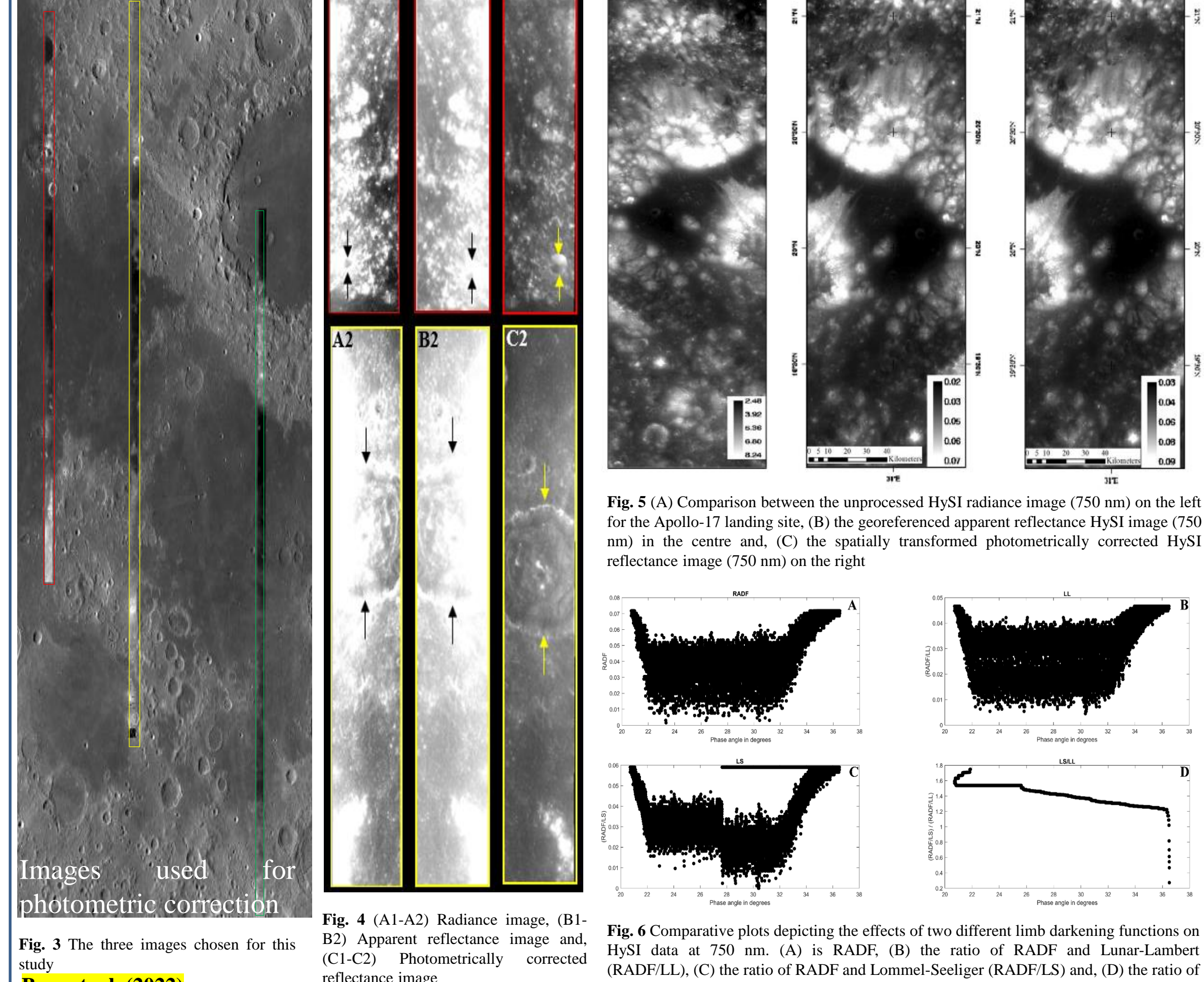


Fig. 5 (A) Comparison between the unprocessed HySI radiance image (750 nm) on the left for the Apollo-17 landing site, (B) the georeferenced apparent reflectance HySI image (750 nm) in the centre and, (C) the spatially transformed photometrically corrected HySI radiance image (750 nm) on the right

A tour of Mars through different orbiter images

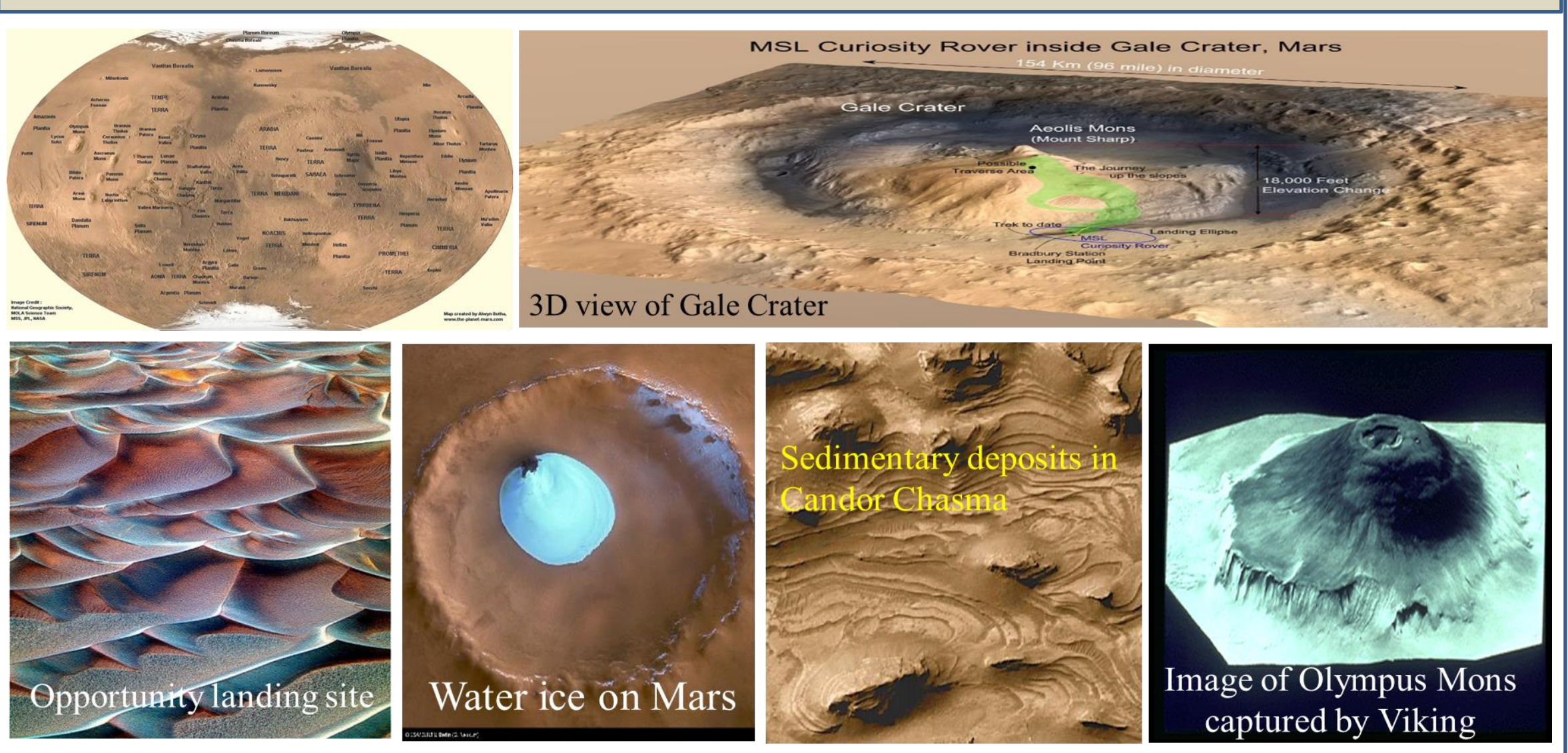


Fig. 1 (a) Gale Crater, Mars (b) Curiosity traverse map showing four locations within Gale Crater – Point Lake (PL), John Klein - Yellowknife Bay (YKB), Cooperstown (CT) and Mt. Remarkable (MR)

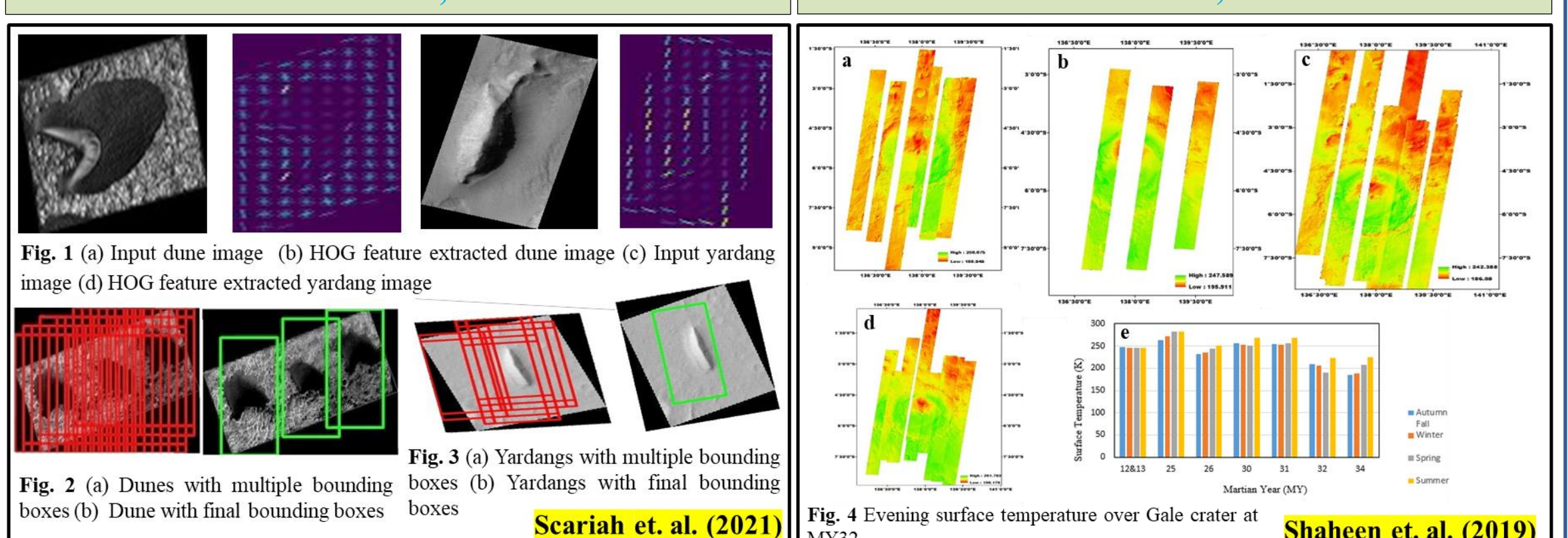


Fig. 2 (a) Dunes with multiple bounding boxes (b) Dune with final bounding boxes

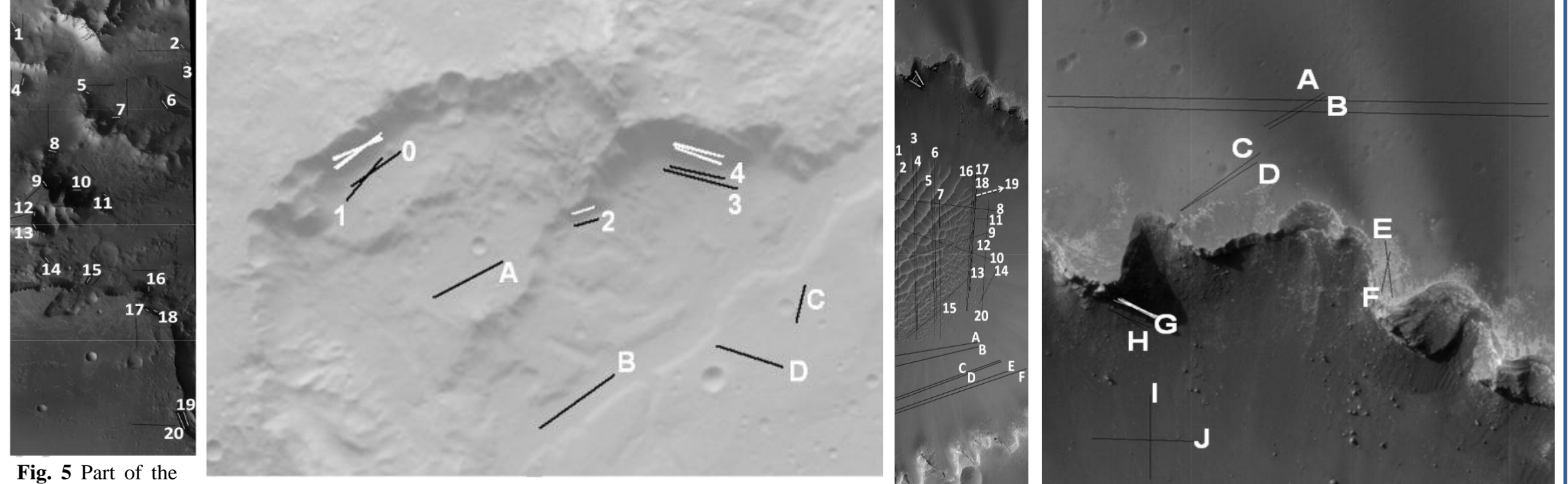


Fig. 3 (a) Yardangs with multiple bounding boxes (b) Yardangs with final bounding boxes

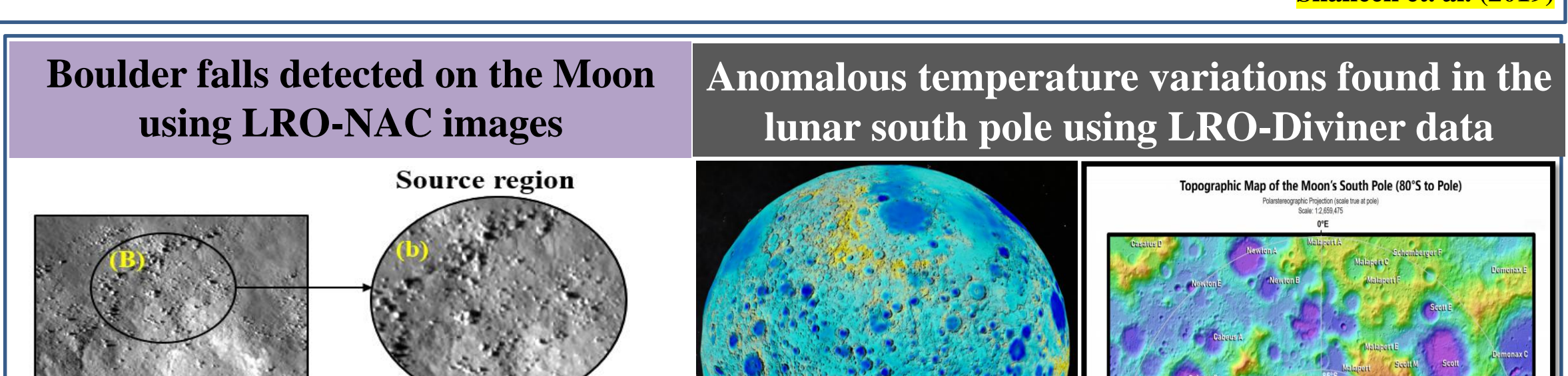


Fig. 4 Evening surface temperature over Gale Crater at MY32

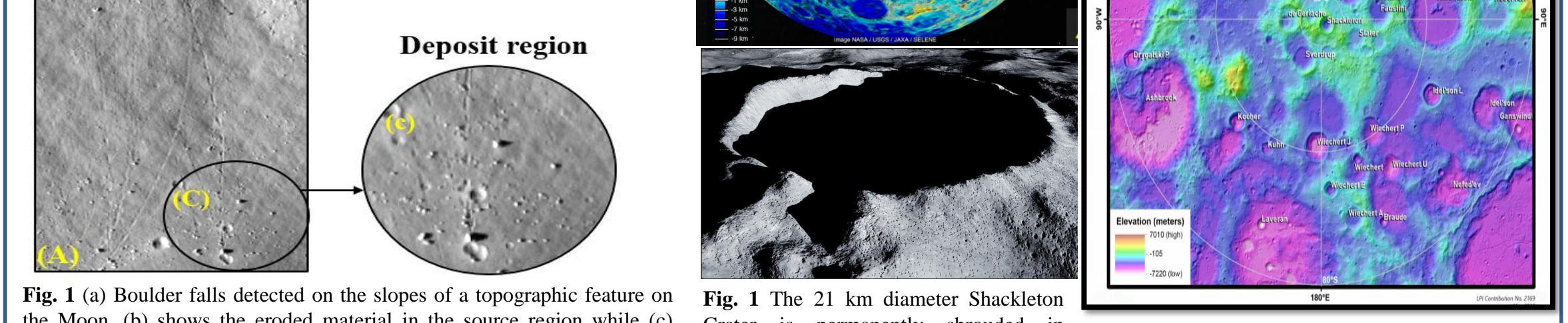


Fig. 5 Part of the HRSC nadir image, A and B yielded 0.38 while C and D yielded 0.40, with an average of 0.39 ± 0.03. Correction factor C = 0.54 and 0.71, respectively.

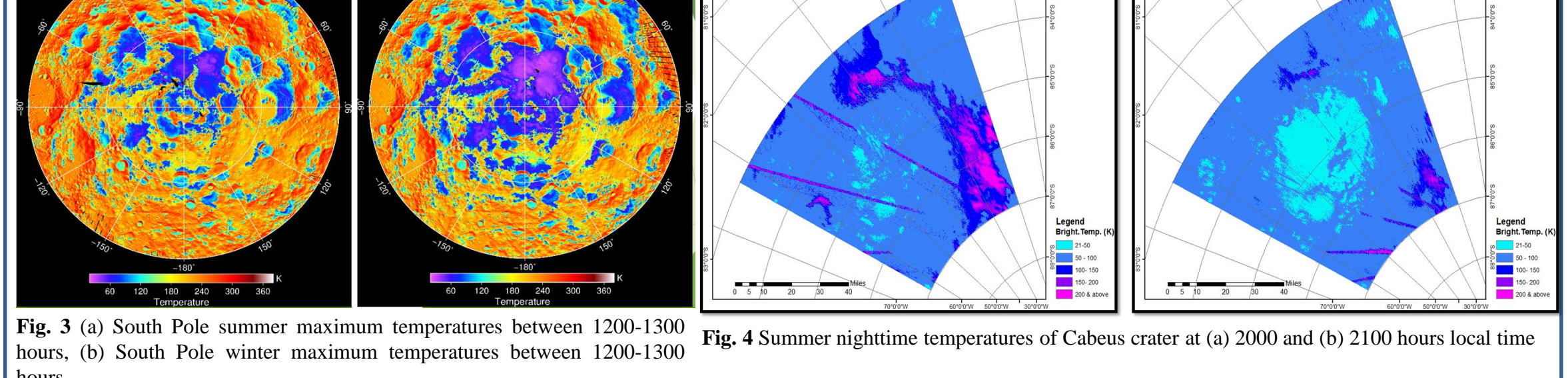


Fig. 6 In the nadir image, A and B yielded 0.38 while C and D yielded 0.40, with an average of 0.39 ± 0.03. Correction factor C = 0.54 and 0.71, respectively.

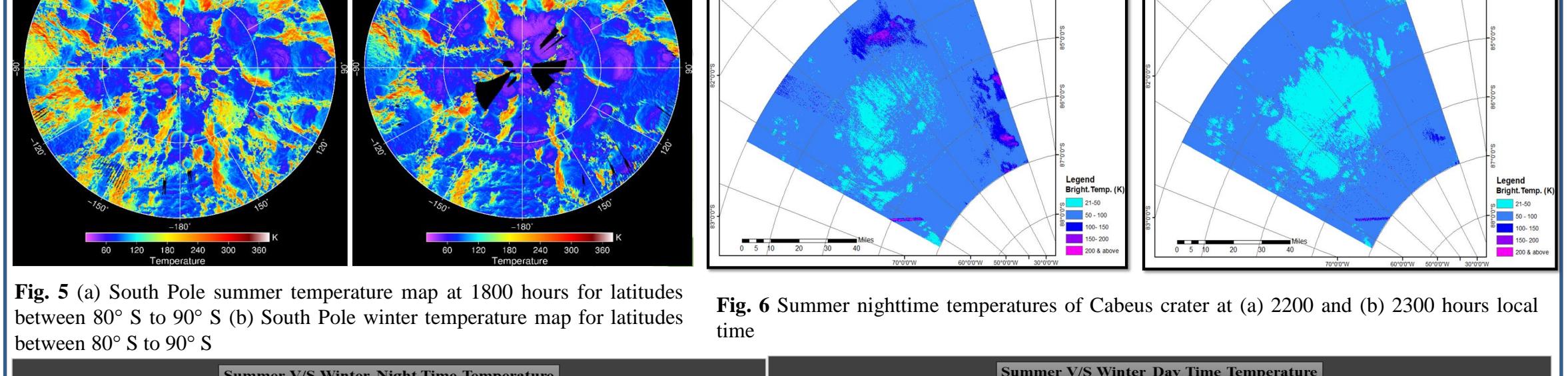


Fig. 7 Victoria Crater, Mars, in a HiRISE red image

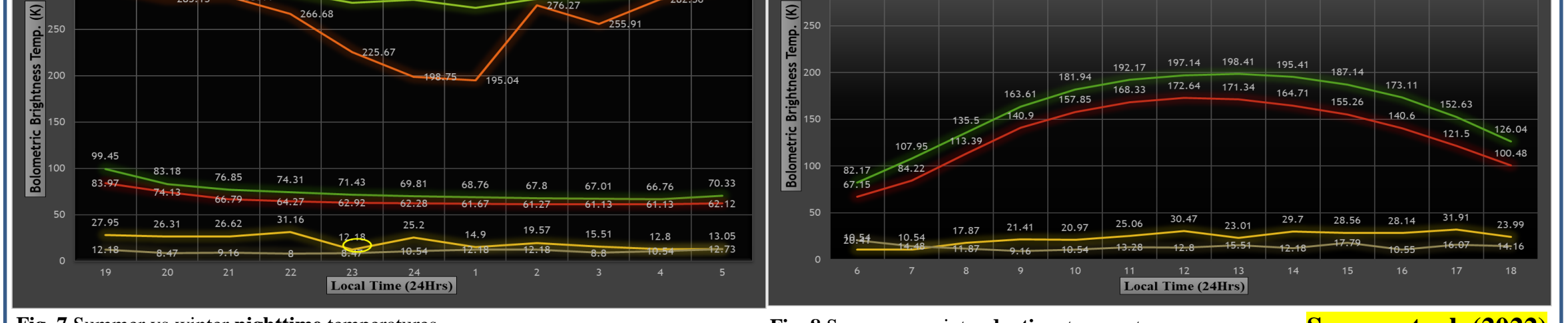


Fig. 8 Summer vs winter nighttime temperatures

Photometric correction of Chandrayaan-1 Hyper-Spectral Imager (HySI) images for the first time

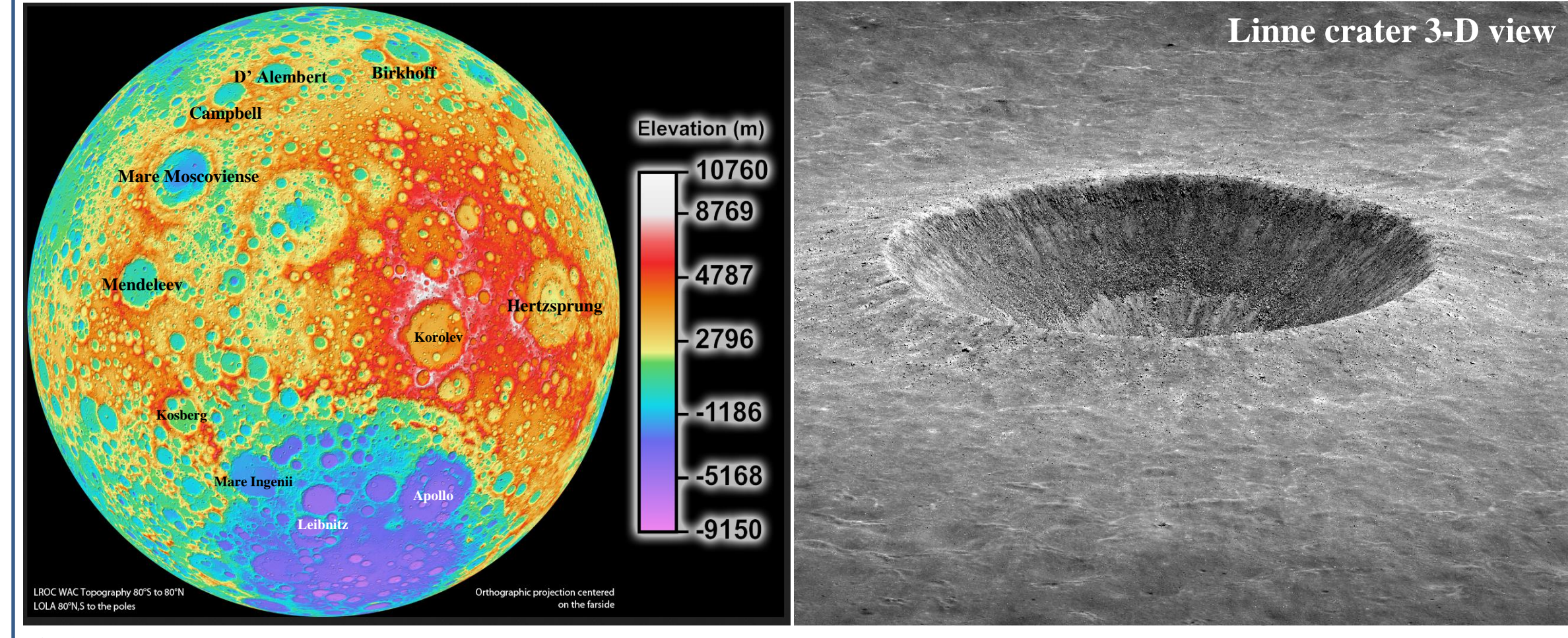


Fig. 1 Hemispherical topographic map of the Moon

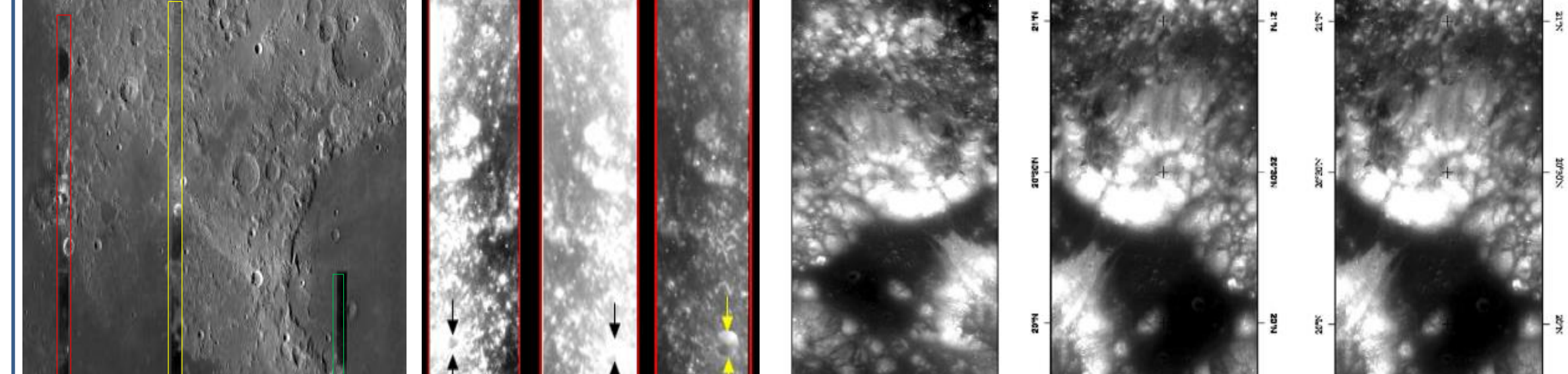


Fig. 2 3-D view of Linne Crater, Moon

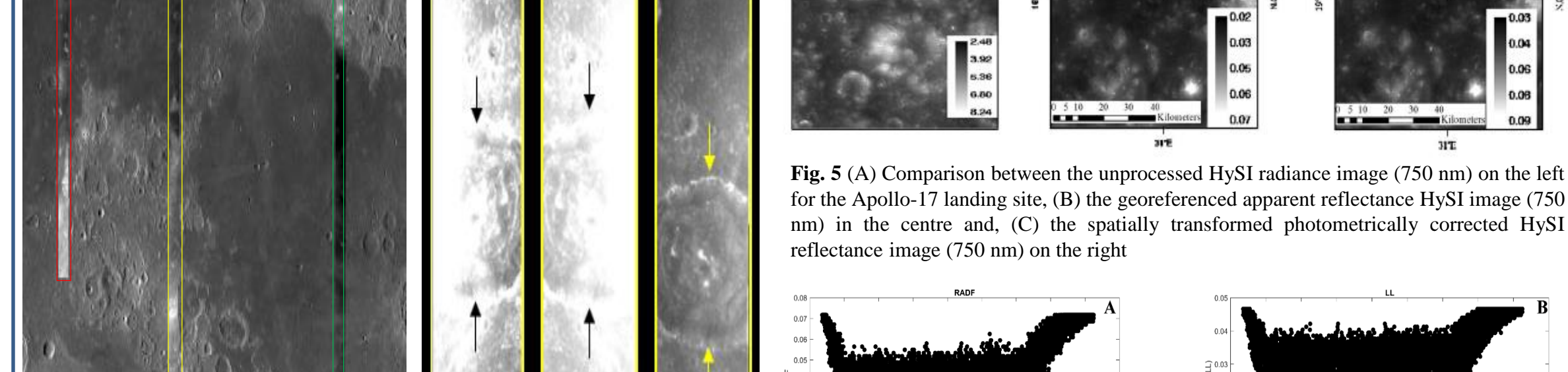


Fig. 3 The three images chosen for this study

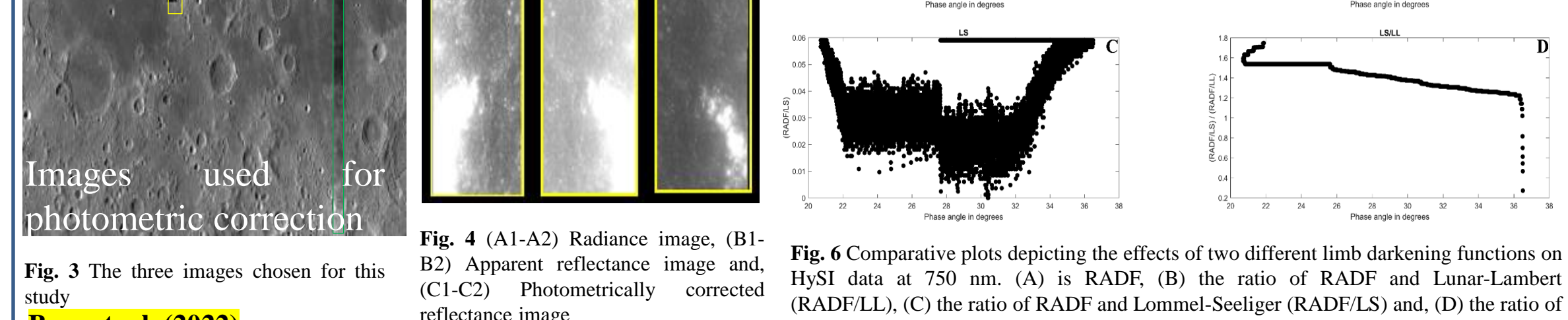


Fig. 4 (A1-A2) Radiance image, (B1-B2) Apparent reflectance image and, (C1-C2) Photometrically corrected reflectance image

Boulder falls detected on the Moon using LRO-NAC images

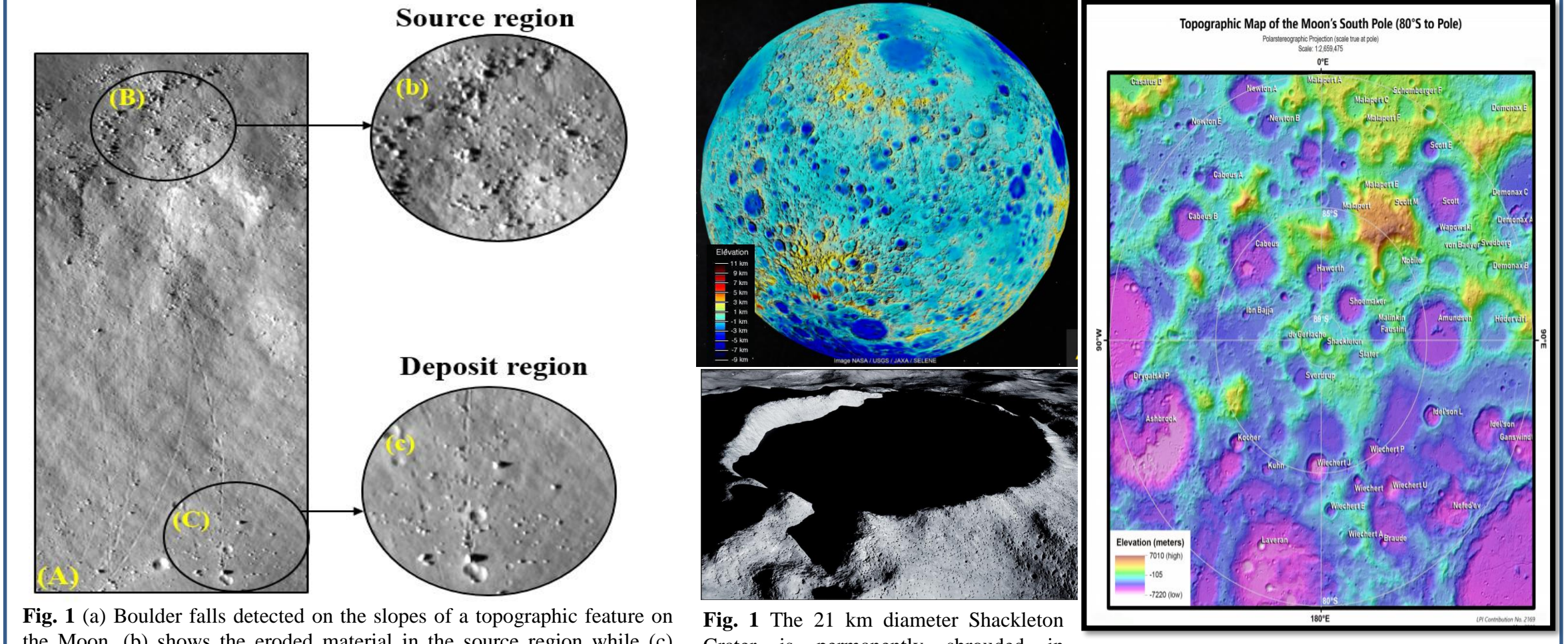


Fig. 1 (a) Boulder falls detected on the slopes of a topographic feature on the Moon, (b) shows the eroded material in the source region while (c) shows boulders getting deposited downslope

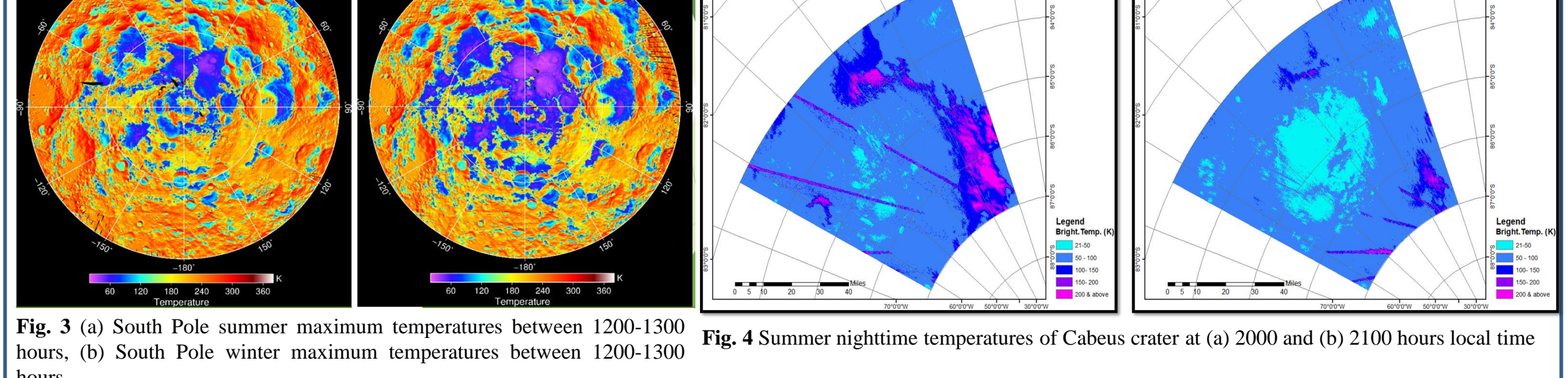


Fig. 2 Topographic map of the lunar South Pole

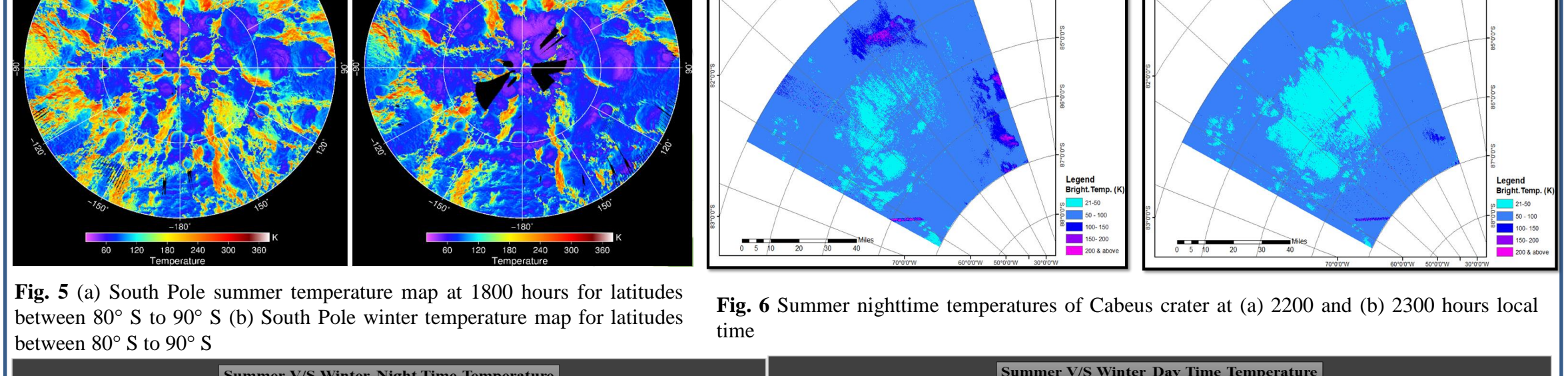


Fig. 3 Summer vs winter nighttime temperatures

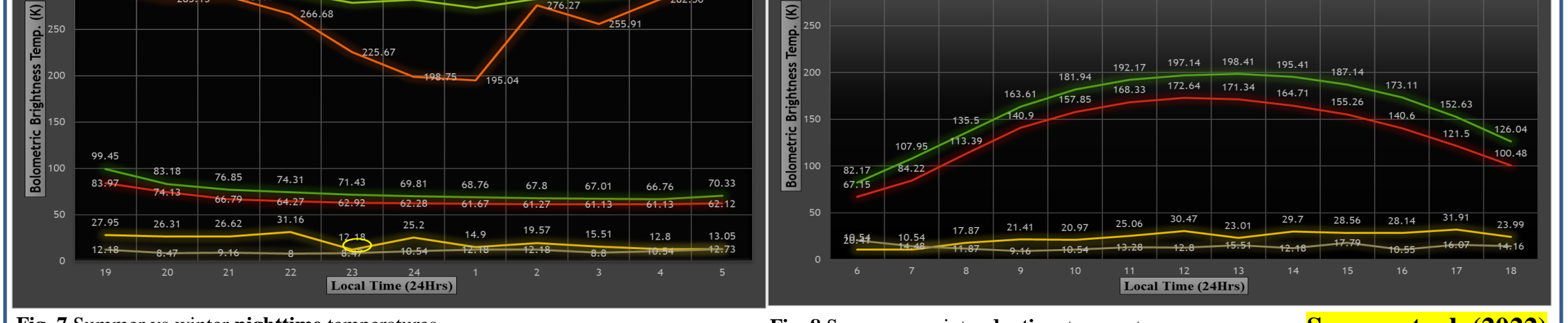


Fig. 4 Summer vs winter daytime temperatures